

RSC Advances



This is an *Accepted Manuscript*, which has been through the Royal Society of Chemistry peer review process and has been accepted for publication.

Accepted Manuscripts are published online shortly after acceptance, before technical editing, formatting and proof reading. Using this free service, authors can make their results available to the community, in citable form, before we publish the edited article. This *Accepted Manuscript* will be replaced by the edited, formatted and paginated article as soon as this is available.

You can find more information about *Accepted Manuscripts* in the [Information for Authors](#).

Please note that technical editing may introduce minor changes to the text and/or graphics, which may alter content. The journal's standard [Terms & Conditions](#) and the [Ethical guidelines](#) still apply. In no event shall the Royal Society of Chemistry be held responsible for any errors or omissions in this *Accepted Manuscript* or any consequences arising from the use of any information it contains.

ARTICLE

Supramolecular Self-assembly and Photovoltaic Property of Soluble Fluorogallium Phthalocyanine

Cite this: DOI: 10.1039/x0xx00000x

Jian Zhang,^a Yaowen Li,^a Laibing Wang,^a Michiya Fujiki,^b Xiaopeng Li,^c Zhengbiao Zhang,^a Wei Zhang,^{*:a} Nianchen Zhou^a and Xiulin Zhu^{*:a}Received 00th January 2014,
Accepted 00th January 2014

DOI: 10.1039/x0xx00000x

www.rsc.org/

Within the present work, two soluble phthalocyanine compounds, fluorogallium tetra-*tert*-butylphthalocyanine (ttbPcGaF) and its precursor hydroxygallium tetra-*tert*-butylphthalocyanine (ttbPcGaOH) were successfully synthesized. ttbPcGaF had a much stronger ability than that of ttbPcGaOH to self-organize into well-ordered one-dimensional (1D) supramolecular polymers in solid state by solution coating technique. The photovoltaic properties of ttbPcGaF and ttbPcGaOH as electron donor materials in solution-processed Bulk Heterojunction (BHJ) organic solar cells (OSCs) were investigated, respectively. Due to the retention of the self-assembly property of ttbPcGaF and nanoscale phase separation in the ttbPcGaF:PC₆₁BM blend film, the ttbPcGaF-based BHJ OSC provided a profoundly improved power conversion efficiency (PCE) of 0.41%, as compared with a low PCE of 0.03% afforded by ttbPcGaOH.

Introduction

Because of strongly chemical-thermal stability and a high light-harvesting property in the visible and near-infrared regions, phthalocyanines (Pcs) have been widely investigated for molecule-based electronic and optical devices.¹⁻⁴ The strong inherent π - π stacking interactions between neighboring Pc molecules makes possible to produce supramolecular structures, which exhibits improved photophysical and electronic properties. However, this inherent characteristic of Pcs is often defective owing to the rich adaptability of slippery π - π stacks.⁵ The construction of long-range well-ordered Pc-based supramolecules is a very desirable process to polish up the Pcs' opto-electric properties.⁶⁻⁹ Several approaches were explored to construct supramolecular structures based on Pcs.¹⁰⁻¹⁸ Nolte et al. reported the formation of Pc's columnar aggregates driven by ionic bond interaction between metal salts and crown ether subunits.^{11,12} The donor-acceptor interactions between Pc dimer were also developed to construct long one-dimensional stacks by Torres and Nolte et al.¹⁸ As another useful tool for production of well-defined Pc's supramolecules, metal-ligand interactions established by Kobuke and co-workers was successfully employed to construct entities based on Pcs.¹⁹ In this regard, the complementary coordination between ligand and central metals, such as magnesium(II),¹⁹ zinc(II),²⁰ and ruthenium(II),²¹ have been reported to produce high-order supramolecular arrays. Most recently, we reported the successful construction of Pc's supramolecular polymers from fluoroaluminium tetra-*tert*-butylphthalocyanines (ttbPcAlFs),²² driven by the coordination interaction between F atom and central Al(III) ion existed in the same ttbPcAlF units. On the other hand, the formation of highly ordered Pcs thin film is extremely important when incorporating Pcs into devices. The solution processing methods, especially Langmuir-Blodgett (LB)²³

and spin-coating²⁴ techniques, have been utilized to fabricate soluble Pcs thin film with ordered columnar structures.

The organic solar cells (OSCs) have been considered one of the most promising technology to solve the increasing energy problems worldwide.²⁵⁻²⁷ The most widely investigated type of OSCs is the bulk heterojunction (BHJ) device,^{28,29} in which electron donor materials (conjugated polymers or small molecules) and electron acceptor materials (fullerene derivatives, PC₆₁BM as a representative) mixed together and casted to a thin film as an active photolayer sandwiched. Since PC₆₁BM has a weak absorption of visible light, the donor materials are expected to possess broad and intense absorption in visible and near-infrared regions to fully exploit the solar energy. Besides, the performance of BHJ OSCs is closely correlated to the morphology of active layer. The ordered BHJ morphology with interpenetrating nanoscale networks plays an important role in improving BHJ OSC performance,³⁰ which can be realized by various external treatment methods, such as thermal annealing,³¹ solvent annealing,³² and the use of processing additives.³³ However, diffusion and aggregation of PC₆₁BM usually occurs by the great driving force offered by the external treatment, inducing the degradation of nanoscale BHJ morphology. Therefore, the supramolecular self-assembly technique is considered as an alternative way to achieve well-controlled morphology of active layer.³⁴

In view of intense Q-band located close to near-infrared region in absorption spectrum and strong self-assembly ability, Pcs can be used as the donor materials to construct efficient BHJ devices. Most of highly efficient Pcs-based OSCs are fabricated by vacuum deposition^{35,36} owing to poor solubility of the unsubstituted Pcs in organic solvents. The solution-processing of soluble Pcs for the preparation of Pc-based BHJ OSCs is believed to be a better choice, due to low cost and feasibility for large-scale roll-to-roll production.^{37,38} There are very rare reports³⁹⁻⁴⁴ of solution-processed

Pc-based BHJ OSCs. Pc–fullerene dyads³⁹ or Pc-and fullerene-containing copolymers⁴⁰ gave the BHJ OSCs with low power conversion efficiency (PCE) (below 0.1%). Recently, Pc blends composed of three different Pc derivatives with various absorption bands improved PCE to 0.12%, which is due to the relatively broader absorption regions and suitable energy level alignment of blend than that of each individual.⁴¹ Torres and co-workers reported a BHJ solar cell with dendritic oligothiophene functionalized ruthenium Pc (RuPc) as donor material providing the highest PCE of 1.6% on account of the enhanced absorption region.⁴² Most recently, Palomares and Torres et al. reported that BHJ OSCs and the organic small molecule solar cell with the PCEs of 0.47% and 0.77% were also achieved using water soluble zinc Pc (ZnPc)⁴³ and the symmetrical *tert*-butyl substitutional ZnPc⁴⁴ as donor material, respectively. However, the above reports didn't study the ordered arrangements of Pcs formed by supramolecular self-assembly technique to improve the device performance. The only exception is the BHJ device based on soluble discotic liquid crystalline ZnPc and fullerene reported by Jurow et al.. The liquid crystalline ZnPc could self-assemble into ordered columnar structures in thin film, but the PCE of device was just 0.08%.⁴⁵ Hence, the solution processed BHJ OSCs fabricated by self-organized Pcs with improved performance are needed to be further investigated.

Because the solubility of ttbPcAlF is not sufficient for the requirement of solution-processed OSCs,²² the photovoltaic property cannot be investigated. Therefor, Al was replaced by gallium (Ga) to insert into Pc ring which had similar chemical properties with Al. Herein, we reported the synthesis and optoelectric properties of a soluble fluorogallium tetra-*tert*-butylphthalocyanine (ttbPcGaF) and its precursor hydroxygallium tetra-*tert*-butylphthalocyanine (ttbPcGaOH) for the first time. ttbPcGaF has a better self-assembly ability than ttbPcGaOH due to the presence of infinite Ga-F-Ga interactions. Benefiting from the excellent solubility and strong self-organized ability, solution-processed BHJ OSC was fabricated with ttbPcGaF as a donor and PC₆₁BM as an acceptor material. The ttbPcGaF based BHJ device showed a favorable performance with a PCE of 0.41%, more than ten times of 0.03% afforded by ttbPcGaOH.

Experimental

Materials and methods

4-*tert*-Butylphthalonitrile (99%, TCI), gallium chloride (99%, Sigma-Aldrich), quinoline (99%, TCI) were used as received. Unless otherwise specified, all other chemicals were purchased from Shanghai Chemical Reagents and used as received without any further purification.

¹H NMR spectra were recorded on a Bruker 300 MHz nuclear magnetic resonance (NMR) instrument using CDCl₃ as the solvent and tetramethylsilane (TMS) as the internal standard at ambient temperature. UV-vis spectra were recorded with a Shimadzu UV-3100 spectrophotometer. Both Electrospray Ionization-Mass Spectrometry (ESI-MS) and Electrospray Ionization-Traveling Wave Ion Mobility Mass Spectrometry (ESI-TWIM MS) experiments were performed with a Synapt HDMS G2 quadrupole/time-of-flight mass spectrometer (Waters Corporation) to detect the exact masses of the associating polymers formed by T-DAP9. The sprayed solutions were prepared by dissolving 0.1 mg of sample in 1 mL of chloroform/MeOH (80/20, v/v). Tandem MS experiments combined with TWIM separation was performed in a trap cell (fragmentation before ion mobility separation). All tandem MS studies employed 4–110 eV collisions with argon targets. Data analysis was conducted with the Mass Lynx 4.1 and Drift Scope 2.1

programs from Waters. Transmission electron microscopy (TEM) images were obtained using a TecnaiG220 at 200 kV. Atomic force microscopy (AFM) images were recorded under ambient conditions, using a Veeco Digital Instrument Multimode NanoscopeIIIa operating in the tapping mode regime. The samples were prepared by spin-coating onto glass at 1200 rpm from sample solutions in chlorobenzene. Wide-angle X-ray scattering (WAXS) and grazing incidence small-angle X-ray scattering (GISAXS) measurements were performed on equipment with a SAXSess camera (Anton-Paar, Graz Austria) which is connected with an X-ray generator (Philips) operating at 40 kV and 50 mA employing CuK α radiation ($\lambda = 0.154$ nm). The 1D scattering function ($\log I(q)$) was obtained by integrating the 2D scattering pattern which was recorded on an imaging-plate detector (Perkin Elmer) using SAXSQuant software (Anton-Paar, Graz Austria). The *d*-spacing of a peak is expressed by $2\pi/q$. The films were illuminated at an incidence angle of about 0.2° by the X-rays at 8 keV, so that the X-ray beam could penetrate the entire thickness of the film and only a very small portion of the substrate, minimizing the background scattering from the substrate. The cyclic voltammetry (CV) diagrams of ttbPcGaF and ttbPcGaOH were obtained using *n*-Bu₄NPF₆ as supporting electrolyte in acetonitrile solution with a glass carbon working electrode, a platinum wire counter electrode and an Ag/AgNO₃ reference electrode under N₂ atmosphere. Ferrocene was used as the internal standard. The redox potential of Fc/Fc⁺, which has an absolute energy level of -4.8 eV relative to the vacuum level for calibration, is located at 0.09 V in 0.1 M *n*-Bu₄NPF₆/acetonitrile solution. Hence, the HOMO and LUMO energy levels of ttbPcGaF and ttbPcGaOH were estimated from the $E_{\text{ox}}^{\text{on}}$ and $E_{\text{red}}^{\text{on}}$ values according to the following equations: HOMO = -e ($E_{\text{ox}}^{\text{on}} + 4.71$) (eV) and LUMO = -e ($E_{\text{red}}^{\text{on}} + 4.71$) (eV).

Synthesis

ttbPcGaCl

4-*tert*-butylphthalonitrile (2.00 g, 10.8 mmol), gallium chloride (0.53 g, 3.0 mmol), and quinoline (10 mL) were added to the 100 mL of round-bottom flask. The mixture was refluxed at 230 °C for 3 h, cooled to room temperature, and added to the 200 mL of 4 M HCl solution. Some blue particles appeared in the solution, filtered and dried in a vacuum overnight. The obtained product (1.20 g, 52.8%) was used without purification in the following step.

ttbPcGaOH

A portion of the crude ttbPcGaCl (200 mg, 0.237 mmol), 28% ammonia solution (20 mL), and pyridine (15 mL) were refluxed for 7 h. The crude product was obtained by filtration, washed with conc NH₃aq and hot water repeatedly, and purified using column chromatography (silica gel, chloroform/methanol = 30/1 (v/v)). The isolated product was dried at 70 °C for 3 h in a vacuum to yield 180 mg (90%). ¹H NMR (300 MHz, CDCl₃) δ 9.55-8.86 (m, 8H), 8.41-8.08 (m, 4H), 1.96-1.68 (m, 36H).

ttbPcGaF

To a PFA conical flask was added ttbPcGaOH (100 mg, 0.12 mmol), 48% hydrofluoric acid (10 mL). The mixture was stirred at 70 °C for 7 h, filtered through PTFE membrane, and washed with a water/methanol mixture (1/1, v/v). The isolated product was obtained by drying at 70 °C for 3 h under vacuum

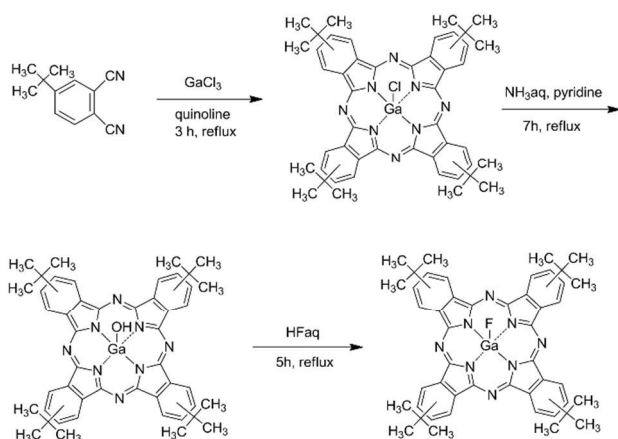
to yield 80 mg (80%). $^1\text{H NMR}$ (300 MHz, CDCl_3) δ 9.57-9.18 (m, 8H), 8.41-8.28 (m, 4H), 1.95-1.70 (m, 36H).

Device fabrication and characterizations

The active layer contained a blend of ttbPcGaF or ttbPcGaOH as electron donor and PC_{61}BM as electron acceptor was prepared from the corresponding solution (10 mg/mL of ttbPcGaF or ttbPcGaOH) in chlorobenzene (ttbPcGaF or ttbPcGaOH: PC_{61}BM = 1:1.5, w/w) by. After spin coating the blend from solution at 1200 rpm, the device was completed by evaporating a 0.8 nm LiF layer protected by 100 nm of Al at a base pressure of 4×10^{-4} Pa. The effective photovoltaic area defined by the geometrical overlap between the bottom ITO electrode and the top cathode was 12 mm^2 . Current-voltage characteristics of the solar cells in the dark and under illumination of 100 mW/cm^2 white light from a Hg-Xe lamp filtered by a Newport 81094 Air Mass Filter, using a GWinStek SFG-1023 source meter. Monochromatic light from Hg-Xe lamp (Newport 67005) in combination with monochromator (Oriel, Cornerstone 260) was modulated with amechanical chopper. The response was recorded as the voltage over a 50Ω resistance, using a lock-in amplifier (Newport 70104 Merlin). A calibrated Si cell was used as reference. All the measurements were performed under ambient atmosphere at room temperature.

Results and discussion

Fluorogallium tetra-*tert*-butylphthalocyanine (ttbPcGaF) was synthesized through three steps as presented in Scheme 1. Introducing *tert*-butyl group to Pc ring could highly improve the solubility of Pc in common organic solvents as well as permit an effective electron tunneling interaction of the interchain Pc solid.⁴⁶ Hence, ttbPcGaF and ttbPcGaOH obtained were highly soluble in 1, 2-dichloroethane (DCE), tetrahydrofuran (THF), chloroform and dichloromethane, and partly soluble in *n*-hexane and methanol, but insoluble in water.



Scheme 1 The synthetic routes of ttbPcGaOH and ttbPcGaF.

Electrospray ionization (ESI) mass spectrometry coupled with traveling wave ion mobility (TWIM) separation^{47,48} was employed to analyze the supramolecular self-assembly of ttbPcGaOH and ttbPcGaF for the first time. TWIM-MS enables mass-, charge-, and shape-dependent dispersion to resolve isomers with distinct

architectures as well as to differentiate the isotope patterns of overlapping charge distributions.⁴⁷⁻⁴⁹ In this regard, π - π stacking

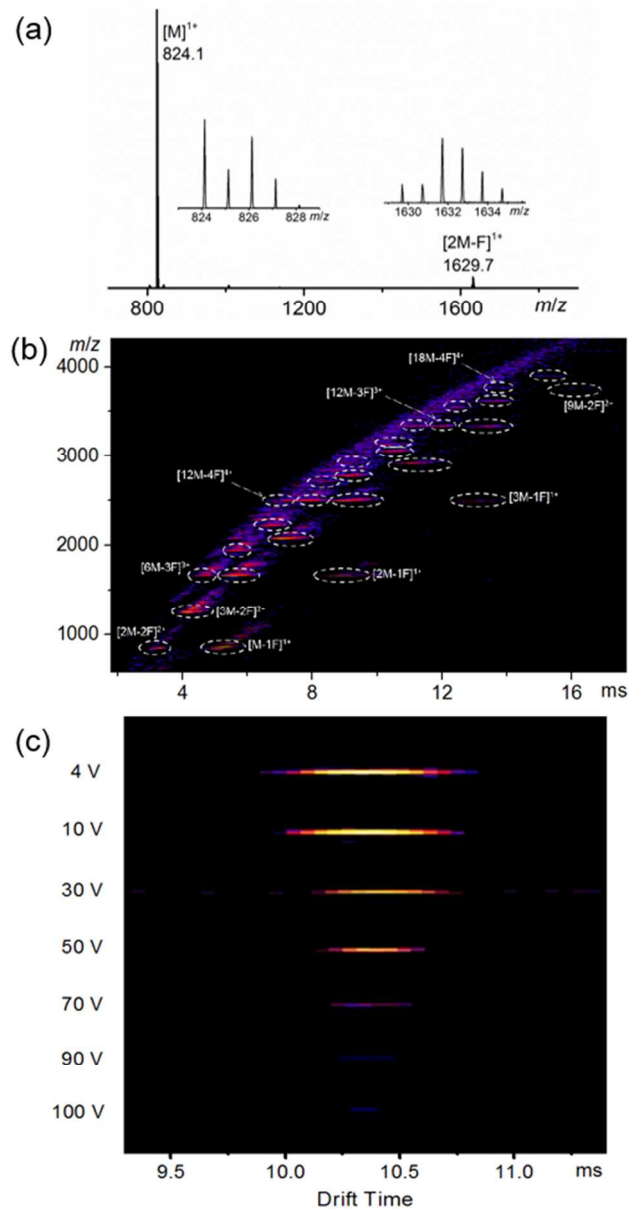


Fig. 1 (a) Conventional ESI and (b) two-dimensional ESI-TWIM mass spectra of ttbPcGaF. (c) Two-dimensional $g\text{MS}^2$ TWIM plot of $[2\text{M}-\text{F}]^+$ at $m/z = 1629.7$. Collisionally activated dissociation took place in the trap cell (before ion mobility separation) at different energies, which was varied by raising the potential applied to the trap from 4 to 100 V. The ions exiting the trap were subsequently separated in the ion mobility region.

along with hydrogen bonding for ttbPcGaOH and Ga-F coordination bond for ttbPcGaF was responsible for construction of Pc-based supramolecular aggregates, respectively. Because of the low mass resolution under mild separation conditions, charge states are superimposed in conventional ESI-MS spectrum. As shown in Fig. 1a, only the molecular mass ion peak (M^+) of ttbPcGaF and the dimer with the loss of one fluoride as $[2\text{M}-\text{F}]^+$ are observed at m/z 824 and 1629, respectively. With the help of TWIM separation, four

different charge states species (from 1^+ to 4^+) can be detected in TWIM mass spectrum. Furthermore, monomer, dimer, trimer as well as higher molecular weight aggregates of ttbPcGaF were observed in Fig. 1b. Remarkably, the largest identified species is composed of 18 repeating units, which cannot be detected for ttbPcGaOH (Fig. S1). Much more observed repeating units of ttbPcGaF (18) than that of ttbPcGaOH (13) demonstrated the relatively stronger self-assembly ability of ttbPcGaF. Moreover, gradient tandem mass spectrometry (gMS²)⁴⁹ was also firstly used to investigate the bonding strength of adjacent ttbPcGaF units, viz., dimer. In Fig. 1c, with applied collisionally activated disassociation (CAD) energy from 4 V to 100 V, the signal of dimer ($[2M-F]^+$) reduces step by step and almost disappears at 100 V, which corresponds to a center-of-mass collision energy of 2.39 eV. In addition, the signal of ttbPcGaOH dimer ($[2M-OH]^+$) (Fig. S1c) also disappears at 100 V but to give a center-to-mass collision energy of 2.15 eV, which is weaker than that of ttbPcGaF. The above results revealed that the inherent self-organization tendency of ttbPcGaOH and ttbPcGaF. With the aid of Ga-F coordination bonds, ttbPcGaF possesses a much stronger bonding of adjacent units as well as self-assembles into supramolecules with higher repeating units as compared to ttbPcGaOH.

It is well-known that the shape and location of the Q-band is a sensitive probe to illustrate the aggregation properties of Pcs.⁵⁰ Fig. 2 shows the UV-vis absorption spectra of ttbPcGaF in 1, 2-dichloroethane (DCE) solution and the corresponding cast thin film on quartz substrate. The absorption spectrum of ttbPcGaF in DCE shows a typical absorption of monomeric Pcs with an intense Q-band at 693 nm.⁵¹ However, the Q-band absorption of thin film blue-shifted to 623 nm, suggesting that ttbPcGaF could readily self-assemble into cofacial "H-aggregates" in solid state. Furthermore, the absorption region of ttbPcGaF thin film extended from visible to near IR areas (from 500 nm to 800 nm). The similar blue-shift of Q-band from 695 to 650 nm and extended absorption region were also observed for ttbPcGaOH as given in Fig. S2. As compared to blue-shift of Q-band of ttbPcGaOH (~45 nm) (Fig. S2), ttbPcGaF showed more obvious blue-shift of (~70 nm) Q-band as observed in Fig. 2. In addition, the relative ratio of supramolecular aggregates in thin film to Pc monomer in DCE solution existed in ttbPcGaF was much higher than that in ttbPcGaOH as revealed in their corresponding UV-vis spectra. As supported by mass spectrometry results, these evidence demonstrated the supramolecular self-assembly ability of ttbPcGaF was much stronger than that of ttbPcGaOH, when transferring from solution to condensed phase.

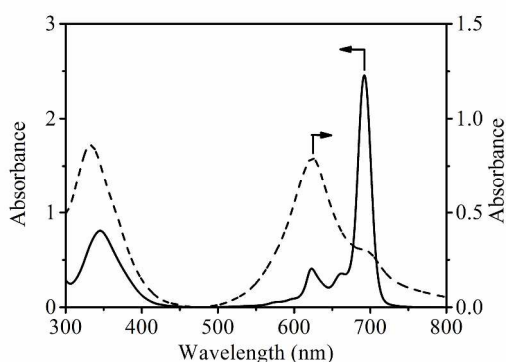


Fig. 2 UV-vis spectra of ttbPcGaF in 1, 2-dichloroethane (solid line) (10^{-5} mol L^{-1}) and the corresponding cast film on a quartz plate (dashed line).

Transmission electron microscopy (TEM) analysis provides an insight into the morphology of supramolecular assemblies.

As expected, the distinct aggregates with diameter of about 20 nm and length of approximate 150 nm were clear observed as presented in Fig. 3. Wide-angle X-ray scattering (WAXS) measurement confirmed that the linear aggregates were 2D arrays of 1D ttbPcGaF-based supramolecular polymer. As shown in Fig. 4, a distinct signal located at 1.78 nm corresponding to the interchain distance of 2D arrays was observed.²² In addition, a broad peak observed at around 0.36 nm was assigned to the average cofacial distance between Pc rings.⁵² For comparison, an analogous lattice image (Fig. S3) was obtained from TEM analysis of ttbPcGaOH film cast from DCE, also revealing a 1D/2D hierarchical structure of ttbPcGaOH-based supramolecular assemblies.

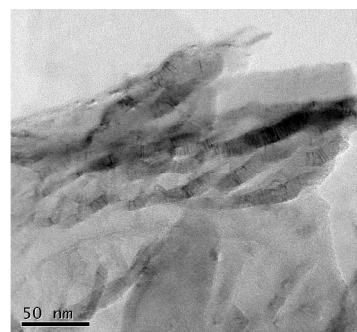


Fig. 3 TEM image of ttbPcGaF casting from a 1, 2-dichloroethane solution (10^{-5} mol L^{-1}).

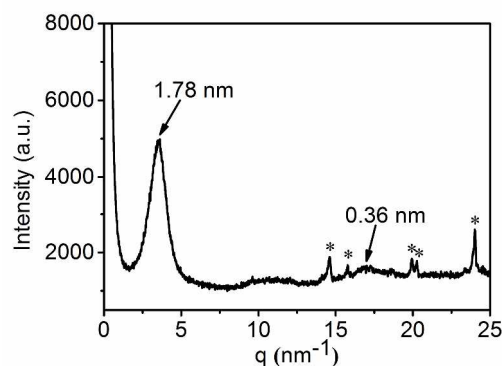


Fig. 4 WAXS profile of ttbPcGaF powder. Asterisk (*) indicates the background peaks of aluminized paper.

Previous studies of Pc-related BHJ OSCs demonstrated that the relatively wide absorption bands could enhance the performance of the corresponding devices. On the other hand, the supramolecular self-assembly technique is an efficient way to achieve well-controlled morphology of active layer, which plays a very important role in improving the device performance. However, there have been very rare reports of Pc-related BHJ OSCs with improving device performance employing the supramolecular self-assembly technique. The only example reported is the ZnPc-based BHJ OSC, in which the liquid crystalline ZnPc formed the ordered columnar structures in thin film. However, the PCE of device was just 0.08%.⁴⁵ The good solubility, the easy construction of supramolecular structures and a tense absorption covered the near-infrared regions encourage us to investigate the photovoltaic property of ttbPcGaF and ttbPcGaOH.

The BHJ OSC was fabricated by a configuration of ITO/PEDOT:PSS/ttbPcGaF:PC₆₁BM/LiF/Al, where ttbPcGaF was used as a donor material and PC₆₁BM as a acceptor material. The

active layer of the solar cell was fabricated by spin-coating a chlorobenzene solution of ttbPcGaF and PC₆₁BM (ttbPcGaF:PC₆₁BM = 1:1.5, w/w). The current-voltage characteristic of the solar cell was given in Fig. 5a. Under white light illumination, the solar cell based on ttbPcGaF:PC₆₁BM exhibited an open circuit voltage (V_{oc}) of 0.60 V, a short circuit current density (J_{sc}) of 1.53 mA/cm², a fill factor (FF) of 0.44, giving rise to a PCE of 0.41%. Fig. 5b shows external quantum efficiency (EQE) spectrum of ttbPcGaF:PC₆₁BM based device. Compared with the absorption spectrum of ttbPcGaF in thin film, the EQE spectrum of the photovoltaic cell shows a similar shape. In addition, the EQE curve exhibited the EQE maximum of 10.6% at 630 nm and a broad response covering from 300 nm to 800 nm, indicating that the generation of charge carriers from absorbed photons is efficient for the current ttbPcGaF-based BHJ OSC. However, the ttbPcGaOH:PC₆₁BM based BHJ OSC showed a dramatically decreased PCE of 0.03% as shown in Fig. S5, which was lower than 1/10 of the ttbPcGaF-based BHJ OSC. The vast different performance should be ascribed to the different charge carrier separation and transportation of active layer resulted from the different supramolecular structures in thin film.

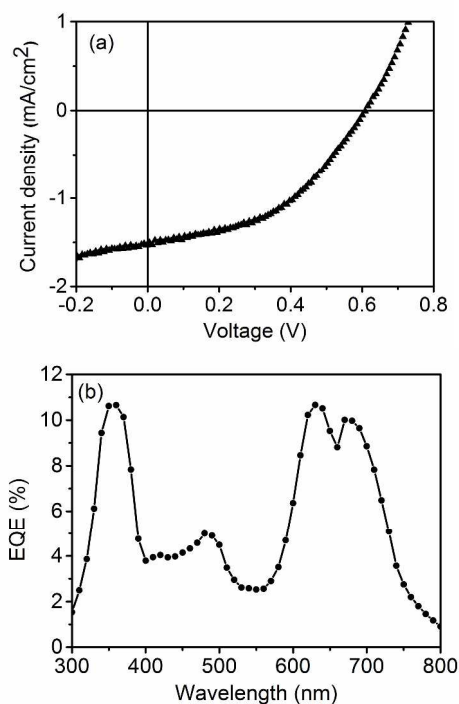


Fig. 5 (a) Current-voltage characteristic of photovoltaic cell prepared from ttbPcGaF:PC₆₁BM under illumination of AM 1.5, 100 mW cm⁻² white light. (b) the corresponding external quantum efficiency (EQE) spectrum of the device.

Fig. 6 shows cyclic voltammetry curves of ttbPcGaF and ttbPcGaOH films. The estimated HOMO/LUMO energy levels of ttbPcGaF and ttbPcGaOH are -4.71/-3.47 eV and -5.05/-3.66 eV, respectively. As an acceptor material, PC₆₁BM possesses the HOMO/LUMO energy level of -3.91/-5.91 eV.⁵³ The energy level offset of LUMO and HOMO between the donor and acceptor materials is the driving force for the exciton dissociation. Hence, the energy level offset should be greater than exciton binding energy (0.3-0.5 eV). Obviously, the difference of LUMO energy levels of ttbPcGaOH and PC₆₁BM (0.25 eV) is not sufficient to overcome the exciton binding energy, which leads to small amount of electron transfer from the donor to the acceptor. In contrast, the energy level

offset of LUMO between ttbPcGaF and PC₆₁BM (0.44 eV) meets the requirements of efficient exciton dissociation. On the other hand, the open circuit voltage (V_{oc}) of organic solar cell is determined by the difference between HOMO level of the donor and LUMO level of the acceptor. Therefore, low-lying HOMO level of the donor is favorable for high V_{oc} . The lower HOMO level of ttbPcGaOH (-5.05 eV) should result a higher V_{oc} than of ttbPcGaF (-4.71 eV). But, as a matter of fact, the V_{oc} of ttbPcGaF-based OSC (0.60 V) is much higher than of that of ttbPcGaOH-based OSC (0.26 V), indicating other effects (phase separation state and the crystallinity) may be mainly determine the performances of ttbPcGaF and ttbPcGaOH-based OSCs.

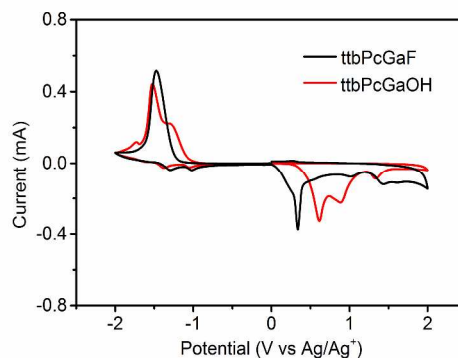


Fig. 6 Cyclic voltammetry curves of ttbPcGaF and ttbPcGaOH films on platinum electrode in 0.1 mol L⁻¹ *n*-Bu₄NPF₆ in CH₃CN solution, at a scan rate of 100 mV s⁻¹.

In order to further investigate the intermolecular interaction of the composites, the TEM, AFM and GISAXS measurements were carried out to study the supramolecular self-assembly behaviours in ttbPcGaF:PC₆₁BM and ttbPcGaOH:PC₆₁BM blend films. As expected, AFM and TEM images (Fig. S6) of ttbPcGaOH:PC₆₁BM blend film revealed serious roughness (RMS = 5.94 nm) and large ttbPcGaOH-enriched domains with sizes ranging from 200 to 500 nm. The larger phase-separated size leads to a smaller interfacial area,⁵⁴ reducing the probability of exciton generation and separation in the blend film of ttbPcGaOH:PC₆₁BM. In contrast, the ttbPcGaF:PC₆₁BM blend film was much more uniform (RMS = 0.50 nm) and nanoscale phase separation could be observed in Fig. 7. The worm-like feature of ttbPcGaF observed in high resolution TEM image (Fig. 7b) indicated that the ttbPcGaF molecules could self-assemble into continuous hole transporting path.⁵⁵ More importantly, the 2D-GISAXS image (Fig. 8) of ttbPcGaF:PC₆₁BM blend film clearly showed a strong diffraction peak at $q_z \approx 3.56 \text{ nm}^{-1}$ assigning to lamellar phase (d -spacing of 1.76 nm). Although there was slight arcing diffraction corresponding to the other lamellar structure, the strong diffraction peak at $q_z \approx 3.56 \text{ nm}^{-1}$ indicated that the worm-like ttbPcGaF domain possessed a relatively higher ordered crystalline molecular arrangement,⁵⁶⁻⁵⁸ which was not interfered by the blend composite of PC₆₁BM. Accordingly, the high PCE of ttbPcGaF:PC₆₁BM based device are attributed to the nanoscale phase separation, predominant ordered crystalline of worm-like domains, which are greatly benefit for the charge separation and transportation. In comparison, disappearance of corresponding diffraction in the ttbPcGaOH:PC₆₁BM blend film (Fig. S7) suggested a low ordered blend film, which also responsible for the relative low PCE value as mentioned above.

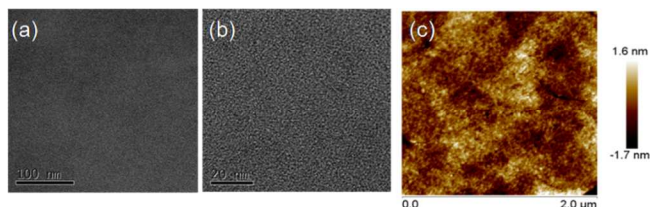


Fig. 7 (a and b) TEM images under varied resolutions and (c) AFM image of ttbPcGaF:PC₆₁BM blend film, RMS (root mean square) = 0.50 nm.

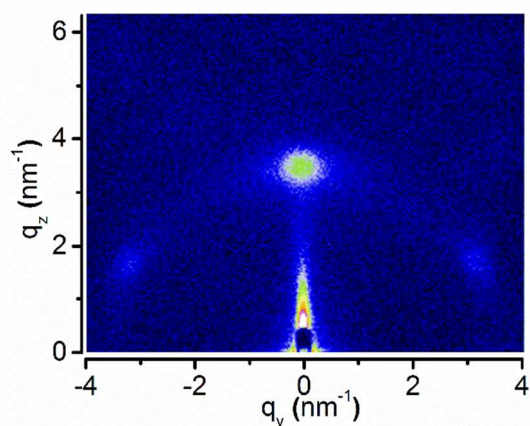


Fig. 8 2D-GISAXS image of ttbPcGaF:PC₆₁BM blend film.

Conclusions

In conclusion, we have successfully synthesized a novel soluble ttbPcGaF and its precursor ttbPcGaOH. The 1D supramolecular polymers were obtained through the well-ordered cofacial stacking of ttbPcGaF with the help of Ga-F coordination bonds and π - π stacking interaction between Pcs. Meantime, ttbPcGaOH can also self-assemble into 1D supramolecular polymers owing to π - π stacking and hydrogen bonding, although the self-organization is somewhat defective. The high solubility in organic solution, the ability of self-assembly in thin film as well as intense absorption at near-infrared regions attract considerable interest for the application of ttbPcGaF and ttbPcGaOH in BHJ OSCs using solution spin-coating technique. Due to the absence of ordered arrangement, and strong aggregation of ttbPcGaOH in ttbPcGaOH:PC₆₁BM blend film, the solution-processed BHJ OSC fabricated with ttbPcGaOH:PC₆₁BM gave a very low PCE of 0.03%. Remarkably, the retention of ordered arrangement of ttbPcGaF and nanoscale phase separation in ttbPcGaF:PC₆₁BM blend film promoted a strong improvement of the PCE to 0.41%. This method, monomers self-assemble into supramolecules to enhance the performance of BHJ OSCs, may afford a new technology to construct high efficient OSCs.

Acknowledgements

The financial support from the Project of International Cooperation of the Ministry of Science and Technology of China (2011DFA50530), the National Nature Science Foundation of China (21104052, 21374072 and 21374068), the Qing Lan Project, the Program of Innovative Research Team of Soochow University and the Project Funded by the Priority

Academic Program Development of Jiangsu Higher Education Institutions (PAPD) are gratefully acknowledged.

Notes and references

^aJiangsu Key Laboratory of Advanced Functional Polymer Design and Application, Department of Polymer Science and Engineering, College of Chemistry, Chemical Engineering and Materials Science, Soochow University, Suzhou, 215123, P. R. China. E-mail: weizhang@suda.edu.cn or xlzhu@suda.edu.cn, Fax/Tel: 0086-512-65882787.

^bGraduate School of Materials Science, Nara Institute of Science and Technology, 8916-5 Takayama, Ikoma, Nara 630-0036, Japan.

^cDepartment of Chemistry and Biochemistry, Texas State University, San Marcos, Texas 78666, United States.

Electronic Supplementary Information (ESI) available: [details of ESI-MS, UV-vis spectra, TEM image, WAXS profile, photovoltaic property of ttbPcGaOH, and TEM, AFM, 2D-GISAXS images of ttbPcGaOH:PC₆₁BM blend film are available in supplementary information]. See DOI: 10.1039/b000000x/

- 1 M. Hanack and M. Lang, *Adv. Mater.*, 1994, **6**, 819.
- 2 G. de la Torre, P. Vázquez, F. Agulló-López and T. Torres, *J. Mater. Chem.*, 1998, **8**, 1671.
- 3 G. de la Torre, P. Vázquez, F. Agulló-López and T. Torres, *Chem. Rev.*, 2004, **104**, 3723.
- 4 M. G. Walter, A. B. Rudine and C. C. Wamser, *J. Porphyrins Phthalocyanines*, 2010, **14**, 760.
- 5 C. C. Leznoff and A. B. P. Lever, *Phthalocyanine: Properties and Applications*, Volume 1–4, VCH, New York 1989/1993/1996.
- 6 G. de la Torre, C. G. Claessens and T. Torres, *Chem. Commun.*, 2007, 2000.
- 7 J. L. Yang, S. Schumann and T. S. Jones, *J. Mater. Chem.*, 2011, **21**, 5812.
- 8 S. Takami, S. Furumi, Y. Shirai, Y. Sakka and Y. Wakayama, *J. Mater. Chem.*, 2012, **22**, 8629.
- 9 M. N. Badrabad, R. Ajeian, S. S. Ardestani, and M. Tavakkoli, *Org. Electron.*, 2012, **13**, 2682.
- 10 T. J. Marks, *Science*, 1985, **227**, 881.
- 11 H. Engelkamp, S. Middelbeek and R. J. M. Nolte, *Science*, 1999, **284**, 785.
- 12 J. A. A. W. Elemans, A. E. Rowan and R. J. M. Nolte, *J. Mater. Chem.*, 2003, **13**, 2661.
- 13 Q. Tang, H. Li, Y. Song, W. Xu, W. Hu, L. Jiang, Y. Liu, X. Wang and D. Zhu, *Adv. Mater.*, 2006, **18**, 3010.
- 14 R. Rai, A. Saxena, A. Ohira and M. Fujiki, *Langmuir*, 2005, **21**, 3957.
- 15 Y. Guan, S. Yu, M. Antonietti, C. Böttcher and C. F. J. Faul, *Chem. Eur. J.*, 2005, **11**, 1305.
- 16 M. Ince, M. V. Martínez-Díaz, J. Barberá and T. Torres, *J. Mater. Chem.*, 2011, **21**, 1531.
- 17 J. Kan, Y. Chen, J. Gao, L. Wan, T. Lei, P. Ma and J. Jiang, *J. Mater. Chem.*, 2012, **22**, 15695.
- 18 A. de la Escosura, M. V. Martínez-Díaz, P. Thordarson, A. E. Rowan, R. J. M. Nolte and T. Torres, *J. Am. Chem. Soc.*, 2003, **125**, 12300.
- 19 K. Kameyama, M. Morusue, A. Satake and Y. Kobuke, *Angew. Chem. Int. Ed.*, 2005, **44**, 4763.
- 20 L. Wu, Q. Wang, J. Lu, Y. Bian, J. Jiang and X. Zhang, *Langmuir*, 2010, **26**, 7489.
- 21 M. S. Rodriguez-Morgade, T. Torres, C. Atienza-Castellanos and D. M. Guldi, *J. Am. Chem. Soc.*, 2006, **128**, 15145.
- 22 W. Zhang, K. Ochi, M. Fujiki, M. Naito, M. Ishikawa, K. Kaneto, W. Takashima, A. Saeki and S. Seki, *Adv. Funct. Mater.*, 2010, **20**, 3941.
- 23 M. J. Cook, *Pure Appl. Chem.*, 1999, **71**, 2145.
- 24 M. Hassan, H. Li and N. B. Mckeown, *J. Mater. Chem.*, 2000, **10**, 39.
- 25 S. Gunes, H. Neugebauer and N. S. Sariciftci, *Chem. Rev.*, 2007, **107**, 1324.
- 26 A. W. Hains, Z. Liang, M. A. Woodhouse and B. A. Gregg, *Chem. Rev.*, 2010, **110**, 6689.
- 27 Y. Lin, Y. Li and X. Zhan, *Chem. Soc. Rev.*, 2012, **41**, 4245.
- 28 Y. Li, Q. Guo, Z. Li, J. Pei and W. Tian, *Energy Environ. Sci.*, 2010, **3**, 1427.
- 29 Y. Li, *Acc. Chem. Res.*, 2012, **45**, 723.

- 30 M. T. Dang, L. Hirsch, G. Wantz and J. D. Wuest, *Chem. Rev.*, 2013, **113**, 3734.
- 31 W. Ma, C. Yang, X. Gong, K. Lee and A. J. Heeger, *Adv. Funct. Mater.*, 2005, **15**, 1617.
- 32 G. Li, V. Shrotriya, J. Huang, Y. Yao, T. Moriarty, K. Emery and Y. Yang, *Nat. Mater.*, 2005, **4**, 864.
- 33 C. Li, Y. Chen, Y. Zhao, H. Wang, W. Zhang, Y. Li, X. Yang, C. Ma, Li. Chen, X. Zhu and Y. Tu, *Nanoscale*, 2013, **5**, 9536.
- 34 P. Zhang, C. Li, Y. Li, X. Yang, L. Chen, B. Xu, W. Tian and Y. Tu, *Chem. Commun.*, 2013, **49**, 4917.
- 35 J. Xue, B. P. Rand, S. Uchida and S. R. Forrest, *Adv. Mater.*, 2005, **17**, 66.
- 36 J. Xue, S. Uchida, B. P. Rand and S. R. Forrest, *Appl. Phys. Lett.*, 2004, **85**, 5757.
- 37 L. Schmidt-Mende, A. Fechtenkötter, K. Müllen, E. Moons, R. H. Friend and J. D. MacKenzie, *Science*, 2001, **293**, 1119.
- 38 S. E. Shaheen, R. Radspinner, N. Peyghambarian and G. E. Jabbour, *Appl. Phys. Lett.*, 2001, **79**, 2996.
- 39 M. A. Loi, P. Denk, H. Hoppe, H. Neugebauer, C. Winder, D. Meissner, C. Brabec, N. S. Sariciftci, A. Gouloumis, P. Vázquez and T. Torres, *J. Mater. Chem.*, 2003, **13**, 700.
- 40 A. de la Escosura, M. V. Martínez-Díaz, T. Torres, R. H. Grubbs, D. M. Guldi, H. Neugebauer, C. Winder, M. Drees and N. S. Sariciftci, *Chem. Asian. J.*, 2006, **1–2**, 148.
- 41 A. Varotto, C-Y. Nam, I. Radivojevic, J. P. C. Tomé, J. A. S. Cavalerio, C. T. Black and C. M. Drain, *J. Am. Chem. Soc.*, 2010, **132**, 2552.
- 42 M. K. R. Fischer, I. López-Duarte, M. M. Wienk, M. V. Martínez-Díaz, R. A. J. Janssen, P. Bäuerle and T. Torres, *J. Am. Chem. Soc.*, 2009, **131**, 8669.
- 43 J. W. Ryan, E. Anaya-Plaza, A. de la Escosura, T. Torres and E. Palomares, *Chem. Commun.*, 2012, 48, 6094.
- 44 A. Sánchez-Díaz, R. Pacios, U. Muñecas, T. Torres and E. Palomares, *Org. Electron.*, 2011, **12**, 329.
- 45 M. J. Jurov, B. A. Hageman, E. DiMasi, C. Nam, C. Pabon, C. T. Black and C. M. Drain, *J. Mater. Chem. A*, 2013, **1**, 1557.
- 46 J. M. Warman, J. Piris, W. Pisula, M. Kastler, D. Wasserfallen and K. Müllen, *J. Am. Chem. Soc.*, 2005, **127**, 14257.
- 47 X. Ren, B. Sun, C. Tsai, Y. Tu, S. Leng, K. Li, Z. Kang, R. M. V. Horn, X. Li, M. Zhu, C. Wesdemiotis, W. Zhang and S. Z. D. Cheng, *J. Phys. Chem. B.*, 2010, **114**, 4802.
- 48 N. Lou, Y. Wang, X. Li, H. Li, P. Wang, C. Wesdemiotis, A. P. Sokolov and H. Xiong, *Macromolecules*, 2013, **46**, 3160.
- 49 X. Li, Y. Chan, G. R. Newkome and C. Wesdemiotis, *Anal. Chem.*, 2011, **83**, 1284.
- 50 W. J. Schutte, M. Sluyters-Rehbach and J. H. Sluyters, *J. Phys. Chem.*, 1993, **97**, 6069.
- 51 G. de la Torre, M. Nicolau and T. Torres, In *Phthalocyanines: Synthesis, Supramolecular Organization and Physical Properties (Supramolecular Photosensitive and Electroactive Materials)*; Nalwa, H. S., Ed.; Academic Press: New York, 2001.
- 52 M. Kimura, H. Ueki, K. Ohta, H. Shirai and N. Kobayashi, *Langmuir*, 2006, **22**, 5051.
- 53 Y. He, Y. Li, *Phys. Chem. Chem. Phys.*, 2011, **13**, 1970.
- 54 Y. Liang and L. Yu, *Acc. Chem. Res.*, 2010, **43**, 1227.
- 55 P. Wu, G. Ren and S. A. Jenekhe, *Macromolecules*, 2010, **43**, 3306.
- 56 H. J. Kim, J. W. Kim, H. H. Lee, T. Kim, J. Jang and J. Kim, *J. Phys. Chem. Lett.*, 2011, **2**, 1710.
- 57 H. J. Kim, J. W. Kim, H. H. Lee, B. Lee and J. Kim, *Adv. Funct. Mater.*, 2012, **22**, 4244.
- 58 H. J. Kim, H. H. Lee, J. W. Kim, J. Jiang and J. Kim, *J. Mater. Chem.*, 2012, **22**, 8881.